Freestanding 3D Mesoporous Co$_3$O$_4$@Carbon Foam Nanostructures for Ethanol Gas Sensing

Lei Li,[†,‡] Minmin Liu,[†,§] Shuijian He,[†,§] and Wei Chen*,[†]

[†]State Key Laboratory of Electroanalytical Chemistry, Changchun Institute of Applied Chemistry, Chinese Academy of Sciences, Changchun 130022, People's Republic of China

[‡]The College of Electrical and Electronic Engineering, Changchun University of Technology, Changchun 130012, People's Republic of China

[§]University of Chinese Academy of Sciences, Beijing 100039, People's Republic of China

ABSTRACT: Metal oxide materials have been widely used as gas-sensing platforms, and their sensing performances are largely dependent on the morphology and surface structure. Here, freestanding flower-like Co$_3$O$_4$ nanostructures supported on three-dimensional (3D) carbon foam (Co$_3$O$_4$@CF) were successfully synthesized by a facile and low-cost hydrothermal route and annealing procedure. The morphology and structure of the nanocomposites were studied by X-ray diffraction, X-ray photoelectron spectroscopy, energy-dispersive spectroscopy, and scanning electron microscopy (SEM). The SEM characterizations showed that the skeleton of the porous carbon foam was fully covered by flower-like Co$_3$O$_4$ nanostructures. Moreover, each Co$_3$O$_4$ nanoflower is composed of densely packed nanoneedles with a length of $\sim$10 μm, which can largely enhance the surface area (about 286.117 m^2/g) for ethanol sensing. Gas sensor based on the as-synthesized 3D Co$_3$O$_4$@CF nanostructures was fabricated to study the sensing performance for ethanol at a temperature range from 180 to 360 °C. Due to the 3D porous structure and the improvement in sensing surface/interface, the Co$_3$O$_4$@CF nanostructure exhibited enhanced sensing performance for ethanol detection with low resistance, fast response and recovery time, high sensitivity, and limit of detection as low as 15 ppm at 320 °C. The present study shows that such novel 3D metal oxide/carbon hybrid nanostructures are promising platforms for gas sensing.
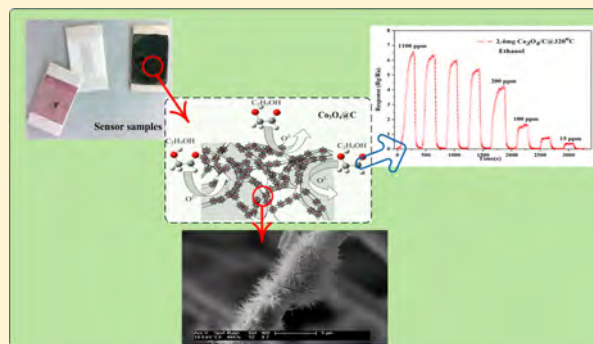
Ethanol sensing has been widely applied in various fields, such as in ethanol breath analyzers for detecting ethanol vapor in the drivers' breath,[1] in foodstuffs experiments to assess the development of bacteria and fungi in food,[2] in monitoring the biomedical and chemical processes in chemical industries and so on.[3] In the past several decades, the application of metal oxide semiconductor (MOS) materials in the field of gas sensors has received widespread attention. One-dimensional spinel cobalt tetroxide (Co$_3$O$_4$) is a kind of p-type semiconductor material which is not only a promising functional material for high-performance supercapacitors,[4,5] anode materials of lithium-ion batteries,[6,7] electrochemical sensors,[8] but also an excellent candidate for gas sensors.[9−11] For instance, Wang et al. synthesized functionalized Co$_3$O$_4$ nanobelt arrays on a Ti foil substrate and studied their application as Li-ion battery anodes.[6] Xiong et al. prepared flower-like quasi-single-crystalline mesoporous Co$_3$O$_4$ nanowire arrays via thermal decomposition, which exhibited enhanced lithium-storage capacity.[7] Guan et al. reported the enhanced capacity and rate capability of the needle-like Co$_3$O$_4$ nanomaterials anchored on graphene sheets.[12] The previous studies showed that Co$_3$O$_4$ nanomaterials are outstanding sensing materials for volatile organic compounds (VOCs)[13,14] and toxic gases.[10] Among the

reported Co$_3$O$_4$ nanomaterials, one-dimensional flower-like Co$_3$O$_4$ is a promising architecture for boosting performance because of their high surface-to-volume ratio and great potential applications in many technological areas. However, flower-like Co$_3$O$_4$ nanomaterials for gas-sensing applications are still scarce. Moreover, the sensing characteristics and mechanism of Co$_3$O$_4$ materials still need to be further elucidated. Meanwhile, the gas-sensing characteristics of one-dimensional Co$_3$O$_4$ materials are greatly affected by their morphology, active surface, dimension, surface-to-volume ratio, and porosity structure, just like other MOS-sensing materials, such as SnO$_2$,[15,16] ZnO$_2$,[17,18] and CuO/Cu$_2$O.[19,20] First, the morphology of Co$_3$O$_4$ materials can affect their exposed crystal surface; in turn, the different exposed surfaces have different sensing responses to target gas.[21−23] Second, by controlling the dimension of Co$_3$O$_4$ nanocomposites, the ratio between crystal surface and volume can be enhanced, which will influence the sensitivity and response intensity of sensing materials.[24] Third, porous nanostructure is beneficial for increasing the diffusion

A   dx.doi.org/10.1021/ac5021613 | Anal. Chem. XXXX, XXX, XXX−XXX

rate of target air, meanwhile enhancing the reaction rate between target gas and Co_3O_4 materials.

Introducing carbon supports into Co_3O_4 sensing materials is an important route to fabricate heterostructures and thus to lower the resistance and improve the gas-sensing performance of sensors. Chen et al. reported the gas sensors based on Co_3O_4-intercalated reduced graphene oxide hybrids, which exhibited good ethanol-sensing performance at room temperature.[25] In another work, it was found that the performance of the CO sensor could be improved by doping 0.1% carbon nanotubes (CNTs) into Co_3O_4–SnO_2 composites.[26] In recent years, three-dimensional (3D) carbon materials have attracted much attention due to their porous structure, high electric conductivity, and large surface area. Their unique structures and properties render them a class of ideal supporting materials. Nowadays, 3D carbon materials have been widely used as supports in energy storage and conversion, electrochemical sensors, etc.[27,28] Our studies showed that the resistance of pure Co_3O_4 is extremely large (over 2 GΩ) at room temperature, and the resistance can decrease to the order of MΩ at higher temperature. Surprisingly, the resistance of carbon-foam-supported Co_3O_4 composites (Co_3O_4@CF) could be decreased to the order of KΩ at room temperature. Therefore, with 3D carbon foam as support, the electron mobility of the composite can be markedly improved.

To the best of our knowledge, an ethanol gas-sensing platform fabricated from freestanding 3D carbon/Co_3O_4 hybrid materials has not been reported yet. In this paper, flower-like Co_3O_4 supported on 3D carbon foam (Co_3O_4@CF) was synthesized by a one-pot hydrothermal treatment of 3D carbon material and cobalt nitrate hexahydrate. Without any surfactant, cobalt oxide nanoneedles tend to assemble into flower-like morphology during the synthetic process. The sensing properties of the Co_3O_4@CF for ethanol gas detection were then studied. The results showed that the 3D hybrids are sensitive to ethanol vapor with a concentration as low as 15 ppm at 320 °C. The present study provides a novel sensing platform for ethanol gas detection.

■ EXPERIMENTAL SECTION

Material Preparation. All reagents were of analytical grade and were used without further purification unless specified. Three-dimensional carbon materials were prepared in advance according to the literature methods.[28] In a typical procedure, 44 mg of $Co(NO_3)_2 \cdot 6H_2O$, 47.5 mg of urea, and 7.5 mg of NH_4F were dissolved in 30 mL of ultrapure water under magnetic stirring for 20 min at room temperature. The prepared freestanding carbon materials were then soaked in the above homogeneous solution for about 8 h. Subsequently, the 3D carbon and the mixed solution were transferred to a 50 mL Teflon-lined stainless steel vessel. The hydrothermal process was performed at 120 °C for 10 h. After being cooled to room temperature, the 3D hybrid materials were washed with nanopure water and ethanol several times and then were dried at 60 °C for several hours. The obtained product was further annealed at 350 °C for 4 h under nitrogen flow. The mesoporous product of carbon-foam-supported Co_3O_4 composites was denoted as Co_3O_4@CF. For comparison, pure unsupported Co_3O_4 nanomaterials were also prepared by following the similar procedure described above without the presence of 3D carbon materials.

Material Characterization. The X-ray powder diffraction (XRD) patterns of precursors and products were obtained on a Bruker D8 Avance X-ray diffractometer with a Cu Kα radiation source (λ = 1.54 Å) between 2θ degree of 10–80°. The X-ray photoelectron spectroscopy (XPS) measurements of samples were recorded on a VG Thermo ESCALAB 250 spectrometer operated at 120 W with pass energy mode at 100 eV. Scanning electron microscopy (SEM), energy-dispersive spectroscopy (EDS), and high-resolution TEM (HRTEM) measurements were carried out on XL30 and JEM-2010(HR) microscopes, respectively. The thermogravimetric analysis (TGA) of the weight percents of Co_3O_4 was carried out on a Pyris Diamond TG/DTA system with operating temperature from room temperature to 800 °C and heating rate of 5 °C/min under air flow. The Brunauer–Emmett–Teller (BET) specific surface area and porosity property analysis of the materials were calculated using an automatic N_2 adsorption/desorption instrument named Quantachrome Autosorb Automated Gas Sorption System.

Sensor Fabrication and Gas-Sensing Measurements. First, different quantities of the Co_3O_4@CF sample (0.4, 2.4, 3.5, and 6 mg) were mixed with N,N-dimethylformamide (DMF) to make homogeneous suspensions. Gas sensors were fabricated by dripping the prepared suspensions on the commercial ceramic substrates with Ag–Pd interdigitated electrodes. The prepared sensors were then dried at 60 °C for several hours in air. The gas-sensing measurements were conducted on a chemical gas sensor-1 temperature pressure (CGS-1TP, Beijing Elite Tech Co., Ltd., China) intelligent gas-sensing analysis system. The resistances of the sensors were recorded at different operating temperatures, which were controlled by the external temperature controller by a heated ceramic plate. The operating temperature could be adjusted from room temperature to 500 °C with the controlling temperature precision of 1 °C. The sensing material (Co_3O_4@CF) was pressed first on the ceramic plate through two metal probes and then preheated about 30 min at the target operating temperature. When the resistance of the sensor reached stability, anhydrous alcohol was injected into the evaporation vessel with a microinjector, and at the same time, the test chamber with 18 L volume was closed. The heating unit for the evaporation vessel and the fans for mixing air and target gas were turned on until the resistance of the sensor reached a constant value. After the measurements, the buttons for heating and mixing the gas atmosphere were turned off and the test chamber was opened to expose the sensor to air. Here, the response of the sensor was defined as the relative change of the resistance of the Co_3O_4@CF material in air and in analytes: $R = R_g/R_a$, where R_a is the resistance of sensor in air, R_g is that in the target gas. The concentration of ethanol gas was calculated by eq 1:

$$Q = \frac{V \times C \times M}{22.4 \times d \times \rho} \times 10^{-9} \times \frac{273 + T_R}{273 + T_B} \tag{1}$$

where Q is the volume of liquid ethanol, V is the volume of the test chamber, C is the concentration of the target gas (ethanol), M is the molecular weight of ethanol, d is the density of liquid ethanol, ρ is the purity of liquid ethanol, and T_B and T_R are the testing and room temperatures, respectively.

■ RESULTS AND DISCUSSION

Characterization of the Co_3O_4@CF Material. For comparison, unsupported Co_3O_4 nanomaterials have also been synthesized with the absence of carbon foam. Figure
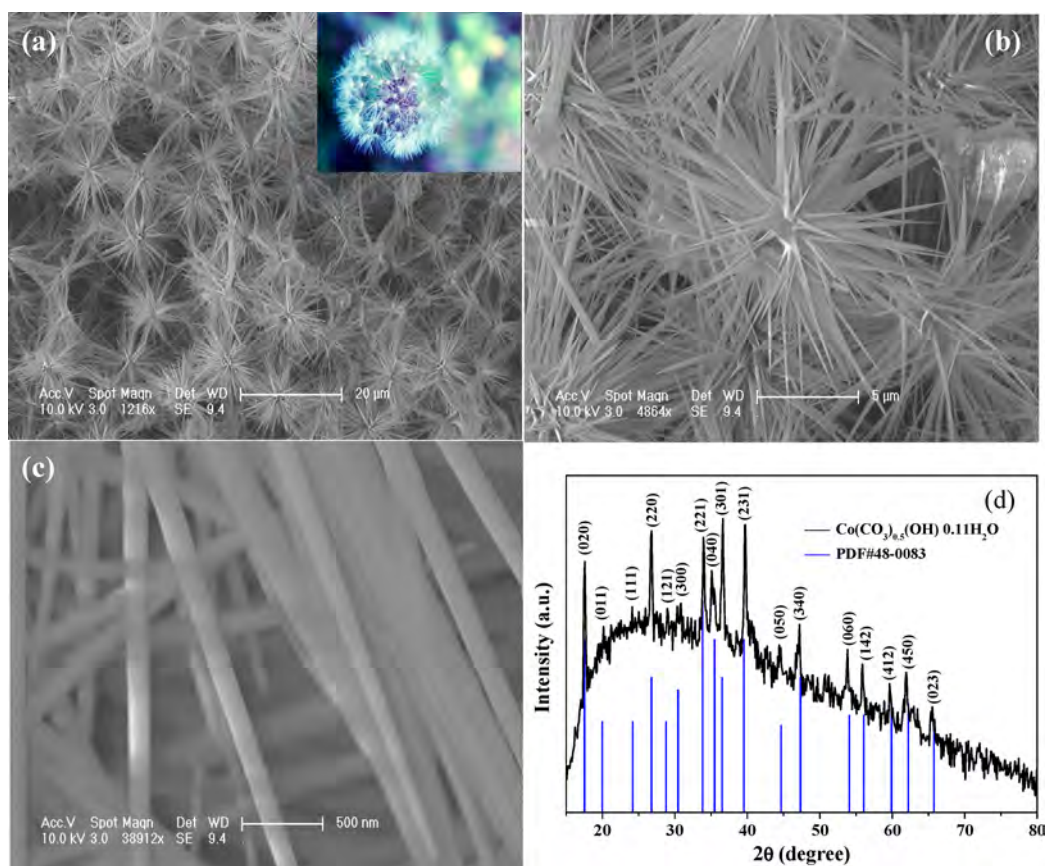
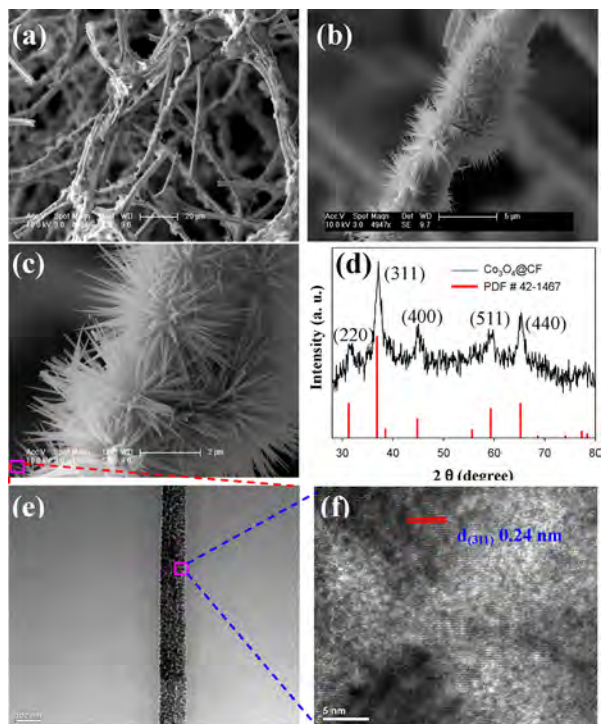**Figure 1.** (a−c) SEM images at different magnifications and (d) XRD pattern of the unsupported product of $Co(CO_3)_{0.5}(OH)\cdot0.11H_2O$ without annealing treatment. Blue lines in d correspond to the JCPDS data of $Co(CO_3)_{0.5}(OH)\cdot0.11H_2O$ (JCPDS card no. 048-0083).

1a−c shows the SEM images of the product after the hydrothermal process but without the annealing treatment. It can be seen that a dandelion-like product was obtained and every branch of the dandelion-like nanomaterials is actually composed of uniform needle-shaped nanostructures just like dandelion "seeds" (Figure 1a). Meanwhile, all nanoneedle structures grow outward along their "cores", appearing as a radial pattern without any curly tendency (Figure 1b). Figure 1a−c indicates that the individual nanoneedle has a length of about 10 μm and a diameter in the range of 80−200 nm. The crystal structure of the product was examined by X-ray diffraction measurement (Figure 1d). By comparing the XRD pattern and the standard JCPDS data of $Co(CO_3)_{0.5}(OH)\cdot$ $0.11H_2O$ (JCPDS card no. 048-0083),[6,7] the unsupported product after the hydrothermal process is pure orthorhombic $Co(CO_3)_{0.5}(OH)\cdot0.11H_2O$.

With the presynthesized carbon foam as support, hybrid materials can be successfully synthesized through the hydrothermal process. The locally magnified SEM images shown in Figure 2a−c clearly confirm that the skeleton of carbon foam could be finely covered by flower-like cobalt hydroxycarbonate. However, compared to the unsupported nanomaterials, the morphology and growth orientation of the $Co(CO_3)_{0.5}(OH)\cdot$ $0.11H_2O$ formed on carbon foam are much different. First, the size of the flower-like structure significantly decreased from ∼15 μm to about 4 μm. At the same time, the length and diameter of the nanoneedles decreased from ∼10 μm and 80− 200 nm to several hundreds and tens of nanometers, respectively. These changes indicate that the carbon foam support also serves as a template to control the growth of the

cobalt-based nanostructures. By depositing sensing materials on 3D freestanding carbon support, the decreased size of cobalt oxide and the porous structures can not only increase the specific surface area but also improve the exposed surface to target gas molecules. Therefore, the 3D porous hybrids can effectively improve the gas-sensing performance, such as sensitivity and limit of detection (LOD),[9,29] which make them very promising as gas-sensing materials.

After being annealed at 350 °C for 4 h in N_2 atmosphere, the as-prepared $Co(CO_3)_{0.5}(OH)\cdot0.11H_2O$ crystals can be converted to pure cobalt oxide (Co_3O_4) phase completely. The crystallographic phase of the oxide was confirmed by the XRD pattern, as depicted in Figure 2d. It can be seen that all the diffraction peaks can be indexed well to the crystal planes of the cubic phase of Co_3O_4 with the lattice constant a = 8.083 Å (JCPDS card no. 42-1467).[30,31] It should be pointed out that the pristine morphology of the cobalt carbonate hydroxide crystals was well preserved in the process of annealing, and no noticeable shape and size change was observed. However, it was found that the surface of the materials became rougher after high-temperature heating, suggesting the generation of some distinct porous structure during the annealing treatment. From the HRTEM images shown in Figure 2e,f, each Co_3O_4 nanoneedle has nanoporous structure which is actually composed of small Co_3O_4 nanoclusters (Figure 2f). As can be seen from Figure 2f, well-resolved lattice fringes with an interplanar spacing of 0.243 nm can be observed in a single nanocluster, corresponding to the (311) plane of Co_3O_4. The formation of nanopores could be ascribed to the accelerated

C

dx.doi.org/10.1021/ac5021613 | Anal. Chem. XXXX, XXX, XXX−XXX

Figure 2. (a−c) SEM images at different magnifications and (d) XRD pattern of the carbon-foam-supported Co_3O_4 nanoflowers ($Co_3O_4@$ CF). For comparison, JCPDS data of bulk Co_3O_4 (JCPDS card no. 42-1467) were also plotted in d (red bars). (e,f) HRTEM images of a single nanoneedle from the Co_3O_4 nanoflowers supported on carbon foam.

decomposition of −OH and −CO_3 during the conversion of $Co(CO_3)_{0.5}(OH)·0.11H_2O$ to Co_3O_4 at high temperature.

To further analyze the composition and chemical states of the flower-like Co_3O_4 nanostructure supported on carbon foam, XPS measurements were also carried out. As shown in Figure 3a, the Co 2p XPS spectrum can be deconvoluted into two major peaks with binding energies at 780.8 and 796.4 eV, corresponding to Co $2p_{3/2}$ and Co $2p_{1/2}$. Meanwhile, the presence of two shakeup satellite peaks located above the two main peaks (786.8 and 801.9 ev) could further confirm the formation of Co_3O_4 crystal phase. The O 1s XPS spectrum could be fitted into three peaks at 531, 532, and 533.3 eV. Among them, the peaks at 531 and 533.3 eV can be assigned to the oxygen from Co_3O_4, and the other one can be ascribed to the adsorbed H_2O molecules by the oxygen species on the surface.[31] The X-ray energy-dispersive spectroscopy analysis (not shown here) also demonstrates that, after high-temperature annealing, the resulting composites mainly contain C, Co, and O (i.e., $Co_3O_4@$CF).

The mass loading of Co_3O_4 on the carbon foam was evaluated by thermogravimetric analysis. Figure 3c shows the TG profile of the $Co_3O_4@$CF composite as a function of heating temperature from 30 to 800 °C at a rate of 10 °C/min. The initial decline of the TG curve below 100 °C corresponds to mass loss of water (6.19 wt %). In the following step, the pyrolysis process of the product shows a sharp drop stage in the TG/DTA profile, which is mainly attributed to the decomposition of carbon skeleton materials.[28,32] Based on the TG/DTA measurements, approximately 80 wt % of the total weight loss is in the temperature range between 250 and 400 °C, suggesting the 20 wt % loading of Co_3O_4 on the carbon foam. The surface area and the pore structure of the $Co_3O_4@$CF were analyzed by the nitrogen sorption technique. The nitrogen adsorption and desorption isotherms of the $Co_3O_4@$CF composites and Co_3O_4 are shown in Figure 3d. From the BET measurements, the specific surface area of the $Co_3O_4@$CF
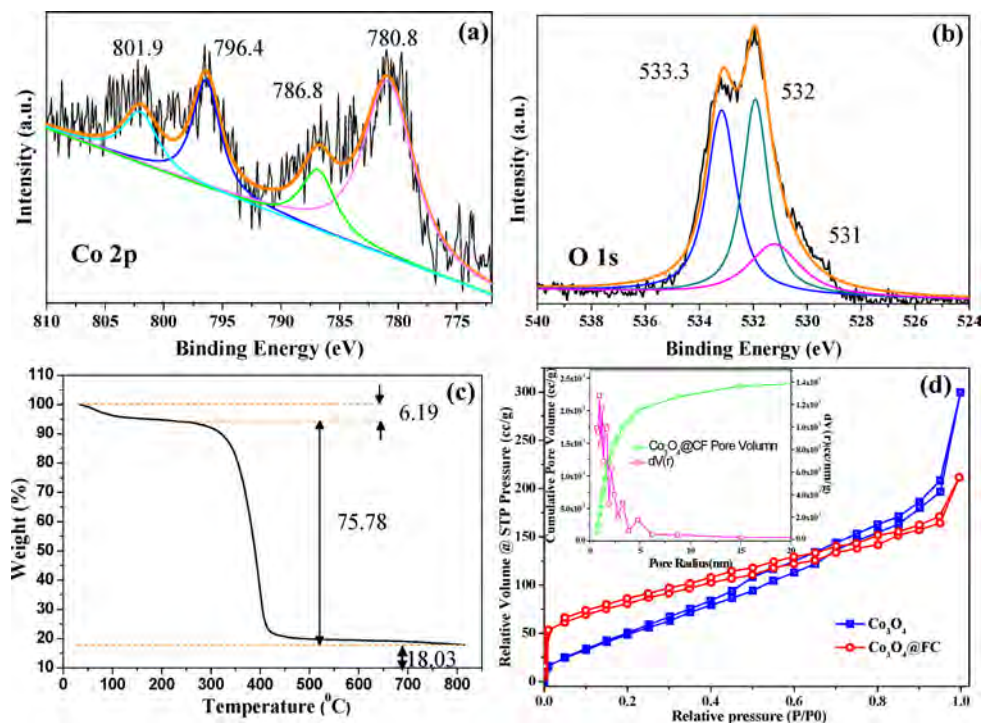
Figure 3. XPS spectra of the $Co_3O_4@$CF: (a) Co 2p, (b) O 1s. (c) TG/DTG profile of the $Co_3O_4@$ CF. (d) Nitrogen adsorption−desorption isotherms for Co_3O_4 and $Co_3O_4@$CF; inset shows the pore size distribution of the $Co_3O_4@$CF.

can reach 286.117 m²/g, which is much higher than that of pure Co_3O_4 (189.083 m²/g). This high value of surface area is favorable for improving the gas-sensing performance of the composites. The pore size distribution of the Co_3O_4@CF based on the Barret−Joyner−Halenda (BJH) method is shown in Figure 3d inset. On the basis of BJH model and desorption data, the average pore radius $dV(r)$ of the hybrid was calculated to be 0.966 nm. The high specific surface area and mesoporous structure of the Co_3O_4@CF composites offer the possibility of efficient interior electron transport and fast gas diffusion, thus resulting in enhanced target gas response.

Sensing Performance of Co_3O_4@CF for Ethanol Gas Detection. The large surface area and porosity structure make the 3D Co_3O_4@CF material promising sensing material for gas detection. Here, the ethanol gas-sensing abilities of the unsupported and supported 3D Co_3O_4 materials were evaluated. In order to obtain the optimum conditions, the effects of operating temperature and mass loading on their sensing performance were first investigated. The responses of Co_3O_4@CF and pure Co_3O_4 with the same mass to 100 ppm of C_2H_5OH were tested as a function of operating temperature. From Figure 4a, it can be seen that the sensing signals increase
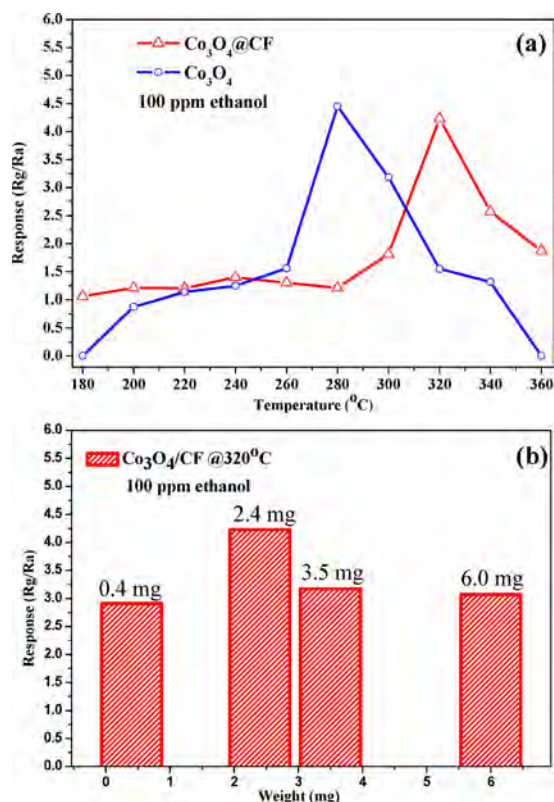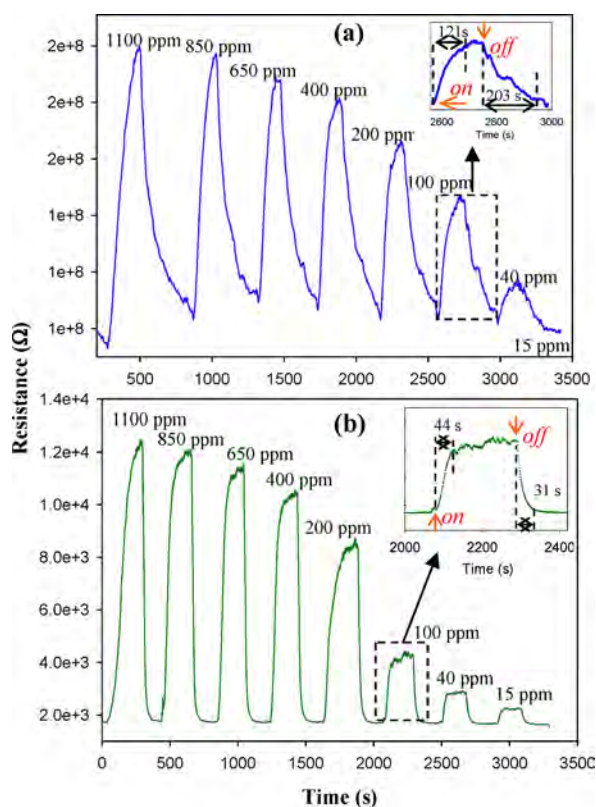

Figure 4. (a) Ethanol gas (100 ppm) response plots as a function of operating temperature on 2.4 mg of Co_3O_4@CF and Co_3O_4. (b) Ethanol gas (100 ppm) response at 320 °C on different quantities of Co_3O_4@CF sensing material.

at the beginning and then decrease with the operating temperature on both samples, with the optimum operation temperatures of 320 and 280 °C, respectively, for the Co_3O_4@CF and unsupported Co_3O_4. At temperatures higher than the optimum ones, the response intensities on both sensors dive sharply, which can be due to the easy desorption of ethanol molecules from the surface of Co_3O_4 or carbon materials.

Compared to the unsupported Co_3O_4, the higher optimum operation temperature for the Co_3O_4@CF heterostructure may be ascribed to the more energy needed to overcome the potential barrier between Co_3O_4 and carbon materials. However, it should be noted that, although only 20 wt % weight loading of Co_3O_4 in the Co_3O_4@CF, the maximum response intensity obtained from the Co_3O_4@CF is very close to that from the pure Co_3O_4 with the presence of 100 ppm ethanol, as shown in Figure 4a. Such results suggest that the Co_3O_4@CF hybrids exhibit higher sensing efficiency due to their unique 3D porous structure and large specific surface area, as displayed in the above BET measurements. The sensing performance change with operation temperature is consistent with those reported from other metal oxide sensors.[10,17]

The mass of Co_3O_4@CF used for the fabrication of the sensor is another important influencing factor for the sensing performance. Here, the sensing properties of the sensors with different quantities of Co_3O_4@CF materials (0.4, 2.4, 3.5, and 6 mg) to 100 ppm ethanol vapor were studied at an operating temperature of 320 °C. It can be seen in Figure 4b that the sensor fabricated with 2.4 mg of Co_3O_4@CF exhibited the highest response intensity among the studied sensors. Based on the result, all of the measurements below are performed on the sensor with the optimized mass (2.4 mg) of Co_3O_4@CF. For gas sensors based on metal oxide semiconductors, their sensing performances are strongly dependent on the initial resistances of the materials. If too little sample is used, the small surface area and insufficient active sites on the surface of the sensing material may show low sensing performance. By increasing the quantity of the sample, the adsorption of target gas on the surface of sensing materials could generate more holes in the valence band of Co_3O_4 and carbon materials, resulting in increased resistance of the p-tpye Co_3O_4@CF-based sensor. However, further increasing the mass of the samples, that is, the thickness of the sensing materials, the target gas molecule can hardly diffuse into the inside of the samples for adsorption. These results suggest that the ethanol gas sensor based on the Co_3O_4@CF hierarchical nanostructures has an optimum loading mass to obtain the best sensing performance.
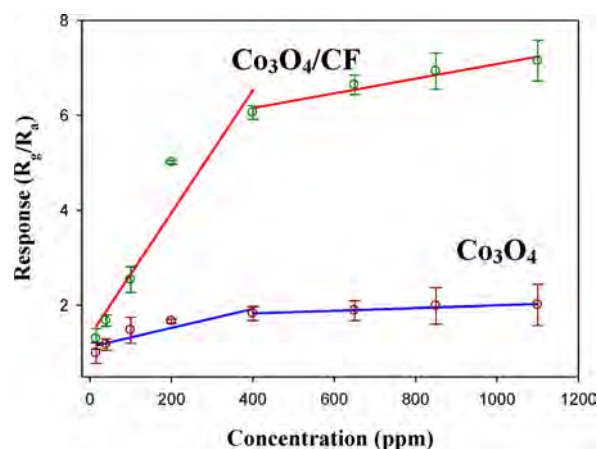
The dynamic ethanol sensing and recovery characteristics of the Co_3O_4@CF and pure Co_3O_4 were further investigated by exposing them to different concentrations of ethanol gas (from 15 to 1100 ppm) and air atmosphere at the optimum operation temperatures (280 and 320 °C). As shown in Figure 5a,b, the resistances of both sensing materials increase with increased ethanol gas concentration, and both sensors show sensitive and reversible response to ethanol gas at different concentrations. Such result suggests that the sensing mechanism of the Co_3O_4 and Co_3O_4@CF corresponds to p-type semiconductor metal oxides. However, by comparing the response plots shown in Figure 5a,b, unsupported Co_3O_4 and Co_3O_4@CF show different ethanol-sensing properties. First, the resistances of these two sensors are extremely different. The resistance of the Co_3O_4@CF is 4 orders lower than that of the pure Co_3O_4 sensor, which could be ascribed to the high electrical conductivity of the 3D carbon foam support in the Co_3O_4@CF. Second, the response and recovery rates of ethanol sensing on the two sensors are much different. On both sensors, the response time increases as the ethanol concentration decreases, which is due to the longer gas diffusion time in the test chamber at lower target gas concentration. However, compared to the pure Co_3O_4, the Co_3O_4@CF shows much faster response and recovery time. As shown in Figure 5a inset,

Figure 5. Ethanol gas-sensing behaviors of (a) Co_3O_4 operated at 280 °C and (b) Co_3O_4@CF operated at 320 °C with different ethanol concentrations (15 to 1100 ppm). The insets in (a) and (b) show the zoomed-in response plots at Co_3O_4 and Co_3O_4@CF, respectively, exposed to 100 ppm ethanol gas.

Figure 6. Response variations of Co_3O_4- (blue curve) and Co_3O_4/CF-based (red curve) sensors as a function of ethanol gas concentration at 320 °C. Solid lines show the linear fitting of the experimental data.

with an ethanol concentration of 100 ppm, the response and recovery times on the Co_3O_4 are 121 and 203 s, respectively, which largely decrease to 44 and 31 s on the Co_3O_4@CF sensor, as shown in Figure 5b inset. Third, by depositing Co_3O_4 on the 3D carbon material, the limit of detection is also improved. By comparing Figure 5a,b, 15 ppm target gas can be hardly detected by the unsupported Co_3O_4, whereas a very obvious sensing signal is observed on the Co_3O_4@CF sensor. From the results above, the 3D Co_3O_4@CF hybrid exhibits enhanced sensing performance for ethanol gas detection compared to pure Co_3O_4. Therefore, based on the sensing measurements shown in Figure 5b, the limit of detection of the 3D Co_3O_4@CF composites for ethanol gas is lower than 15 ppm. Due to the limit of the present gas-distributing system, the LOD of the Co_3O_4@CF sensor will be studied in detail in our future research.

The responses of Co_3O_4 and Co_3O_4@CF sensors to different concentrations of ethanol are depicted in Figure 6. For both sensors, the response intensity increases very rapidly with increasing ethanol concentration at the beginning stage. For the Co_3O_4@CF, with ethanol concentration increasing above 400 ppm, the response tends to rise slowly and saturate at around 1100 ppm. On both sensing materials, the responses (R_g/R_a) increase almost linearly with the ethanol gas concentration in the range of 15−400 ppm. When the p-type material Co_3O_4@CF is exposed in air at high temperature, it would capture oxygen molecules and negatively charged oxygen ions (O^-, O_2^-, and O^{2-}) and free holes (majority carriers) can be formed through the coupling of oxygen molecules with the free

electrons from the Co_3O_4@CF, which results in decreased resistance. With the presence of ethanol gas, due to the large surface area and porous structure of Co_3O_4@CF, the target gas molecule can diffuse to the active sites both on the surface and inside the material. After the adsorption of ethanol molecules, the resistance of the Co_3O_4@CF sensor would increase by consuming holes to recombine electrons released by ethanol gas.[31] As the majority carriers, the density of holes is of significant importance for the gas-sensing performance of sensors based on p-type semiconductor metal oxide.[10,33,34] It should be noted that Figure 6 also demonstrates that the Co_3O_4@CF exhibits much higher sensitivity than the pure Co_3O_4. Meanwhile, compared to some previously reported sensors, our ethanol gas sensor shows better sensing performances with lower resistivity, faster response, and recovery time, likely due to the 3D porous structure and unique properties of the Co_3O_4@CF composites.

■ CONCLUSION

In the present study, 3D freestanding heterostructures with flower-like Co_3O_4 supported on carbon foam were synthesized using a two-step process consisting of a facile hydrothermal route and the subsequent thermal annealing. Due to the high specific surface area and high density of active sites of the 3D porous structure, the Co_3O_4@CF exhibited excellent sensing performance for ethanol detection. Under the optimized conditions, the Co_3O_4@CF composite showed lower resistance, faster response and recovery time, lower detection of limit, and higher sensitivity as an ethanol gas sensor compared to pure Co_3O_4 sensing nanomaterials. Based on the gas-sensing mechanism of the p-type Co_3O_4@CF nanostructures, the gas-sensing performance can be effectively enhanced by increasing the density of holes in the materials. Therefore, the nanostructures fabricated on the 3D and porous carbon foam are promising in gas-sensing applications.

■ AUTHOR INFORMATION

Corresponding Author
*E-mail: weichen@ciac.ac.cn.

Notes
The authors declare no competing financial interest.

■ REFERENCES

(1) Neri, G.; Bonavita, A.; Micali, G.; Donato, N.; Deorsola, F. A.; Mossino, P.; Amato, I.; De Benedetti, B. *Sens. Actuators, B* **2006**, *117*, 196−204.

(2) Ivanov, P.; Llobet, E.; Vilanova, X.; Brezmes, J.; Hubalek, J.; Correig, X. *Sens. Actuators, B* **2004**, *99*, 201−206.

(3) Jones, A. W. Alcohol: Analysis. In *Wiley Encyclopedia of Forensic Science*; John Wiley & Sons, Ltd.: New York, 2009.

(4) Yang, W.; Gao, Z.; Ma, J.; Wang, J.; Wang, B.; Liu, L. *Electrochim. Acta* **2013**, *112*, 378−385.

(5) Liu, X.; Long, Q.; Jiang, C.; Zhan, B.; Li, C.; Liu, S.; Zhao, Q.; Huang, W.; Dong, X. *Nanoscale* **2013**, *5*, 6525−6529.

(6) Wang, Y.; Xia, H.; Lu, L.; Lin, J. *ACS Nano* **2010**, *4*, 1425−1432.

(7) Xiong, S.; Chen, J. S.; Lou, X. W.; Zeng, H. C. *Adv. Funct. Mater.* **2012**, *22*, 861−871.

(8) Mei, W.; Huang, J.; Zhu, L.; Ye, Z.; Mai, Y.; Tu, J. *J. Mater. Chem.* **2012**, *22*, 9315−9321.

(9) Choi, K.-I.; Kim, H.-R.; Kim, K.-M.; Liu, D.; Cao, G.; Lee, J.-H. *Sens. Actuators, B* **2010**, *146*, 183−189.

(10) Patil, D.; Patil, P.; Subramanian, V.; Joy, P. A.; Potdar, H. S. *Talanta* **2010**, *81*, 37−43.

(11) Cao, A.-M.; Hu, J.-S.; Liang, H.-P.; Song, W.-G.; Wan, L.-J.; He, X.-L.; Gao, X.-G.; Xia, S.-H. *J. Phys. Chem. B* **2006**, *110*, 15858−15863.

(12) Guan, Q.; Cheng, J.; Wang, B.; Ni, W.; Gu, G.; Li, X.; Huang, L.; Yang, G.; Nie, F. *ACS Appl. Mater. Interfaces* **2014**, *6*, 7626−7632.

(13) Nguyen, H.; El-Safty, S. A. *J. Phys. Chem. C* **2011**, *115*, 8466−8474.

(14) Lu, Y. Y.; Zhan, W. W.; He, Y.; Wang, Y. T.; Kong, X. J.; Kuang, Q.; Xie, Z. X.; Zheng, L. S. *ACS Appl. Mater. Interfaces* **2014**, *6*, 4186−4195.

(15) Zhou, X.; Fu, W.; Yang, H.; Zhang, Y.; Li, M.; Li, Y. *Mater. Lett.* **2013**, *90*, 53−55.

(16) Sun, P.; Zhou, X.; Wang, C.; Wang, B.; Xu, X.; Lu, G. *Sens. Actuators, B* **2014**, *190*, 32−39.

(17) Zhang, L.; Yin, Y. *Sens. Actuators, B* **2013**, *183*, 110−116.

(18) Shi, L.; Naik, A. J.; Goodall, J. B.; Tighe, C.; Gruar, R.; Binions, R.; Parkin, I.; Darr, J. *Langmuir* **2013**, *29*, 10603−10609.

(19) Volanti, D. P.; Felix, A. A.; Orlandi, M. O.; Whitfield, G.; Yang, D.-J.; Longo, E.; Tuller, H. L.; Varela, J. A. *Adv. Funct. Mater.* **2013**, *23*, 1759−1766.

(20) Zhou, L.; Shen, F.; Tian, X.; Wang, D.; Zhang, T.; Chen, W. *Nanoscale* **2013**, *5*, 1564−1569.

(21) Zhou, K.; Wang, R.; Xu, B.; Li, Y. *Nanotechnology* **2006**, *17*, 3939−3943.

(22) D'Arienzo, M.; Cristofori, D.; Scotti, R.; Morazzoni, F. *Chem. Mater.* **2013**, *25*, 3675−3686.

(23) Wang, L.; Chen, Y.; Ma, J.; Chen, L.; Xu, Z.; Wang, T. *Sci. Rep.* **2013**, *3*, 3500.

(24) Kida, T.; Fujiyama, S.; Suematsu, K.; Yuasa, M.; Shimanoe, K. *J. Phys. Chem. C* **2013**, *117*, 17574−17582.

(25) Chen, N.; Li, X.; Wang, X.; Yu, J.; Wang, J.; Tang, Z.; Akbar, S. A. *Sens. Actuators, B* **2013**, *188*, 902−908.

(26) Wu, R.-J.; Wu, J.-G.; Yu, M.-R.; Tsai, T.-K.; Yeh, C.-T. *Sens. Actuators, B* **2008**, *131*, 306−312.

(27) He, S.; Hu, C.; Hou, H.; Chen, W. *J. Power Sources* **2014**, *246*, 754−761.

(28) He, S.; Chen, W. *J. Power Sources* **2014**, *262*, 391−400.

(29) Deng, S.; Tjoa, V.; Fan, H. M.; Tan, H. R.; Sayle, D. C.; Olivo, M.; Mhaisalkar, S.; Wei, J.; Sow, C. H. *J. Am. Chem. Soc.* **2012**, *134*, 4905−4917.

(30) Jiang, J.; Liu, J. P.; Huang, X. T.; Li, Y. Y.; Ding, R. M.; Ji, X. X.; Hu, Y. Y.; Chi, Q. B.; Zhu, Z. H. *Cryst. Growth Des.* **2010**, *10*, 70−75.

(31) Li, C. C.; Yin, X. M.; Wang, T. H.; Zeng, H. C. *Chem. Mater.* **2009**, *21*, 4984−4992.

(32) Manocha, S. M.; Patel, K.; Manocha, L. M. *Indian J. Eng. Mater. Sci.* **2010**, *17*, 338−342.

(33) Yoon, J.-W.; Choi, J.-K.; Lee, J.-H. *Sens. Actuators, B* **2012**, *161*, 570−577.

(34) Wen, Z.; Zhu, L.; Mei, W.; Li, Y.; Hu, L.; Sun, L.; Wan, W.; Ye, Z. *J. Mater. Chem. A* **2013**, *1*, 7511−7518.

G

dx.doi.org/10.1021/ac5021613 | *Anal. Chem.* XXXX, XXX, XXX−XXX